

Article

Luminescence Efficiency of Cadmium Tungstate (CdWO_4) Single Crystal for Medical Imaging Applications

Christos Michail ^{1,*}, Vaia Koukou ¹, Niki Martini ¹, George Saatsakis ², Nektarios Kalyvas ¹, Athanasios Bakas ³, Ioannis Kandarakis ¹, George Fountos ¹, George Panayiotakis ² and Ioannis Valais ¹

¹ Department of Biomedical Engineering, Radiation Physics, Materials Technology and Biomedical Imaging Laboratory, University of West Attica, Ag. Spyridonos, 12210 Athens, Greece; koukou@uniwa.gr (V.K.); mmartini@uniwa.gr (N.M.); nkalyvas@uniwa.gr (N.K.); kandarakis@uniwa.gr (I.K.); gfoun@uniwa.gr (G.F.); valais@uniwa.gr (I.V.)

² Department of Medical Physics, Faculty of Medicine, University of Patras, GR-15310 Rion, Greece; gsaatsakis@upatras.gr (G.S.); panayiot@upatras.gr (G.P.)

³ Department of Biomedical Sciences, University of West Attica, Ag. Spyridonos, 12210 Athens, Greece; abakas@uniwa.gr

* Correspondence: cmichail@uniwa.gr; Tel.: +30-210-5385-387

Received: 25 April 2020; Accepted: 26 May 2020; Published: 27 May 2020



Abstract: Background: In this study, the light output of a cadmium tungstate (CdWO_4) single crystal was measured under various X-ray radiographic energies. Methods: A CdWO_4 single crystal ($10 \times 10 \times 10 \text{ mm}^3$) was exposed to X-rays in the 50–130 kVp range. Measurements were evaluated against published data for single crystals of equal dimensions ($\text{CaF}_2:\text{Eu}$ and $\text{Lu}_3\text{Al}_5\text{O}_{12}:\text{Ce}$). Since the crystal was examined for application in medical imaging detectors, the emitted optical spectrum was classified with respect to the spectral compatibility of numerous commercial optical sensors. Results: The luminescence efficiency (LE) was found to constantly increase with X-ray energy and was higher than that of $\text{CaF}_2:\text{Eu}$ for energies above 90 kVp. However, the efficiency of the previously published $\text{Lu}_3\text{Al}_5\text{O}_{12}:\text{Ce}$ was found to be constantly higher than that of CdWO_4 . The light emitted from CdWO_4 can be optimally detected by certain charge-coupled devices (CCDs), amorphous silicon photodiodes, and photocathodes. Conclusions: The high density (7.9 g/cm^3) of CdWO_4 and the luminescence signal of this material make it suitable for medical imaging (such as dual energy), high-energy physics or for applications of scintillators in harsh environments.

Keywords: scintillators; crystals; radiation sensors; medical detectors; CdWO_4

1. Introduction

Cadmium tungstate (CdWO_4 or CWO) is a scintillator with a long history as an energy converting medium. CdWO_4 attracted scientists' attention due to its unique internal properties (Table 1) [1]. The first scientist who investigated properties regarding luminescence for this material was Kroger [2]. CdWO_4 is one of the denser scintillating materials ($\rho = 7.9 \text{ g/cm}^3$), with one of the shortest radiation lengths of 10.6 mm and exceeds about 30% to 50% of the light output of sodium iodide doped with thallium (NaI:Tl) [2–12]. The attenuation coefficients of this material are very high, and the light yield has been reported to range from 6200 to 28,000 photons/MeV depending upon the crystal defects [6,8,13–18]. The emission of CdWO_4 covers a wide band with the main peak at 490 nm, which is ideal for coupling with a variety of sensors, such as photomultiplier tubes (PMTs) and silicon photodiodes (Si) [4,7,19–22]. The reported energy resolution varies from 7.5% to 8.5% using

Cs-137 gamma radiation ($E_\gamma = 662$ keV) [6,16]. Furthermore, CdWO_4 is a non-hygroscopic, radiation hard, cheap material, with short values of afterglow (0.05% after three milliseconds of exposure), a high effective atomic number (Z_{eff} values ranging from 61 to 66 were reported in the literature), and a gamma ray detection efficiency ($\rho Z^4 \text{eff}$) equal to 134×10^6 [1,3,4,7,8,13,14,18,23–26]. However, there are certain drawbacks such as the fact that it is difficult to produce in large dimensions and it is toxic due to cadmium [16,25–30]. These properties make CdWO_4 suitable for various applications, such as high-energy physics, spectroscopy, gamma-ray detectors, as well as in the search for dark matter in the universe, neutrinoless 2β decay detection, and α decay of ^{180}W experiments [8,31].

CWO has been also used in photoelectrochemical (PEC) water-splitting sensors, optical fibers, introscopy, photocatalysis, radiometric devices, lasers, electronics, and photovoltaics [10–12,22,31,32]. Furthermore, CdWO_4 has a high melting point (1272 °C) which is ideal for applications in harsh environments such as in industrial applications for nondestructive testing (NDT) of welds on pipelines and pressure vessels in the oil and gas industry, in dual-energy non-intrusive inspection of cargo containers, in deep geology boreholes, in marine research and nuclear plants [3,4,6,10–12,30,33,34].

Furthermore, it has been used for dosimetric applications and as an X-ray scintillator in medical imaging, especially in computed tomography (CT), in conjunction with charge-coupled devices (CCDs), silicon photodiodes or photomultiplier tubes [1,3,4,6,7,13,14,16,18,25–29,35–38]. Regarding CT, CWO has more attractive properties (afterglow, temperature coefficient, X-ray detection, radiation hardness) than cesium iodide activated with thallium (CsI:Tl), which was initially used [9,15].

In the current study a CdWO_4 single crystal was examined in the energy range employed in X-ray imaging, in order to be integrated into sensors used in medical imaging such as in dual-energy imaging detectors using novel methodologies [39–42].

Table 1. CdWO_4 , $\text{CaF}_2:\text{Eu}$, and $\text{Lu}_3\text{Al}_5\text{O}_{12}:\text{Ce}$ crystal properties [1,3,4,6–8,13–18,23–25,43–47].

Properties	CdWO_4	$\text{CaF}_2:\text{Eu}$	$\text{Lu}_3\text{Al}_5\text{O}_{12}:\text{Ce}$
Wavelength (Max. Emission—nm)	490	435	535
Wavelength Range (nm)	380–800	395–525	475–800
Decay Time (ns)	5000	950	70
Light-Yield (photons/MeV)	6200–28,000	13,000–30,000	16,000–27,000
Photoelectron Yield (% of NaI(Tl))	30–50	50	20
Radiation-Length (cm)	1.06	3.05	1.3
Refractive Index	2.2–2.3 (@max nm)	1.47 (@435 nm)	1.84 (@633 nm)
Density (g/cm^3)	7.9	3.18	6.73
Atomic Number (Effective)	61–66	16.5	62.9
Melting Point (°K)	1325	1360	2020
Coefficient of Thermal Expansion (1/C)	10.2×10^{-6}	19.5×10^{-6}	8.8×10^{-6}
Conductivity (Thermal, W/mK)	4.69(@300K)	9.7	9.6
Hardness (Mohs)	4–4.5	4	8.5
Hygroscopic	No	No	No

To this aim, the output signal of CdWO_4 under X-ray excitation was recorded and compared with data for other materials ($\text{CaF}_2:\text{Eu}$ and $\text{Lu}_3\text{Al}_5\text{O}_{12}:\text{Ce}$), of the same dimensions and thickness (10 mm \times 10 mm \times 10 mm). CdWO_4 was selected (i) because it had a light yield (LY) value of 28 photons/keV, higher than that of $\text{Lu}_3\text{Al}_5\text{O}_{12}:\text{Ce}$ (25 photons/keV) which was recently examined by our group [47] and was found to have high luminescence efficiency values, and (ii) due to the fact that it is a cheap material [44,45]. The spectrum of emitted light was also studied for its compatibility with the optical sensitivities of various optical sensors.

2. Materials and Methods

For the experiments, a CdWO_4 single crystal was used (Advatech) [45] with dimensions of 10 mm \times 10 mm \times 10 mm. The surfaces of the crystal were polished. The X-ray tube (BMI, Merate, Curno, Italy) that was used for the X-ray measurement was operated in the voltage range from 50 to 130 kVp.

In the output of the X-ray tube, an aluminum filter was added (thickness 20 mm) in order to consider the attenuation of the incident X-ray spectrum by a typical human chest [48].

2.1. Output Luminescence Signal

During X-ray excitation, the energy flux (power per unit of area) of luminescence light emitted by the crystal was measured by placing the crystal sample in the input port of a sphere that integrates the incident light, in order to correct for crystal light output spatial and angular distribution irregularities (Oriel 70451) [49]. The light at the output port was collected by a PMT connected to an electric current meter (Model 6430 Keithley Instruments Inc., Cleveland, OH, USA) [50]. Light energy flux data were divided by the corresponding incident X-ray exposure rate (\dot{X}) data (at each tube voltage) directly measured via an RTI Piranha P100B wireless digital multimeter. By combining the energy flux of light ($\dot{\Psi}_\lambda$) (emitted by the crystal) with the exposure rate incident on the detector, the output signal luminescence efficiency (LE) of the sample can be obtained using the following Equation (1):

$$\eta_A(kVp) = \dot{\Psi}_\lambda(kVp) / \dot{X} \quad (1)$$

where $\eta_A(kVp)$ is LE at a particular X-ray tube voltage, expressed in efficiency units (EU) ($\mu\text{W} \times \text{m}^{-2} / (\text{mR} \times \text{s}^{-1})$).

2.2. Scintillator/Sensor Spectral Matching and Effective Luminescence Efficiency

Every optical sensor can detect to a different degree the optical photons produced by a scintillator. The degree of overlapping between the spectral response $SD(\lambda)$ of the sensor and the optical spectrum distribution of photon fluence $\phi_L(\lambda)$ produced by the scintillator can be quantified by a factor expressing the spectral matching, as follows (2) [51,52]:

$$\alpha_s = \frac{\int_{\Delta\lambda} \phi_L(\lambda) S_D(\lambda) d\lambda}{\int_{\Delta\lambda} \phi_L(\lambda) d\lambda} \quad (2)$$

A high-resolution HR2000 spectrometer (Ocean Optics Inc., Largo, FL, USA) was used to measure crystals' light, excited at 312 nm by a Vilber Lourmat (VL-215M, Paris, France) ultraviolet (UV) lamp. The spectral response of various optical detectors that are used in a large number of medical applications was obtained from manufacturers' data [53–56]. The effective luminescence efficiency (η_{eff}) between the output signal of the scintillator and the spectral response of various sensors was estimated by multiplying the luminescence efficiency with the spectral matching factor [51].

2.3. Energy-Absorption Efficiency (EAE)

The scintillator's general detection and absorption characteristics can be quantified using the quantum detection efficiency (QDE) and the energy absorption efficiency (EAE). QDE is the fraction of incident photons attenuated by the detector material and is traditionally used to evaluate detection properties of all detector types; however, it is more suitable for photon-counting devices (e.g., those used in nuclear medicine). On the other hand, in most applications of X-ray detection, the output signal is proportional to the total energy absorbed in the detector material. Thus, EAE, being equal to the fraction of energy deposited within the scintillator mass [51,52], is of particular interest.

To calculate EAE, the ratio of the mass energy absorption coefficient over the total mass attenuation coefficient is required:

$$EAE(E) = \frac{\int_0^{E_0} \Phi_0(E) E \left(\frac{\mu_{tot,en}(E)}{\mu_{tot,t}(E)} \right) (1 - e^{-(\mu_{tot,t}(E)/\rho)W}) dE}{\int_0^{E_0} \Phi_0(E) E dE} \quad (3)$$

$\Phi_0(E)E$ is the X-ray photon fluence (photons per unit of area) incident on the scintillator, multiplied by the corresponding energy (E), giving the incident X-ray energy fluence. $\mu_{tot,t}(E)/\rho$ is the X-ray total mass attenuation and $\mu_{tot,en}(E)/\rho$ is the total mass energy absorption coefficient. W denotes crystal thickness.

The coefficient of energy absorption represents the average fraction of the kinetic energy of secondary charged particles that is locally deposited in the detector mass [57]. The coefficients of total attenuation and energy absorption of CdWO_4 were obtained from the National Institute of Standards and Technology (NIST) data regarding cadmium (Cd), tungsten (W) and oxygen (O) using the XmuDat photon attenuation database software [57–60].

3. Results

The variation of the CdWO_4 's LE with X-ray energy is shown in Figure 1, for X-rays from 50 to 130 kVp. Results were compared with data for $\text{CaF}_2:\text{Eu}$ and $\text{Lu}_3\text{Al}_5\text{O}_{12}:\text{Ce}$ crystals ($10 \times 10 \times 10 \text{ mm}^3$) [46,47]. The LE values showed a tendency to increase, with both CdWO_4 and $\text{Lu}_3\text{Al}_5\text{O}_{12}:\text{Ce}$ crystals within the examined energy range following a similar trend. However, for the examined samples (preparation method, impurity levels, etc.), CdWO_4 values were in all cases lower than those of $\text{Lu}_3\text{Al}_5\text{O}_{12}:\text{Ce}$, from 9.65% to 16.95%. On the other hand, $\text{CaF}_2:\text{Eu}$ showed a plateau at 80 kVp (luminescence efficiency equal to 22.22 Efficiency Units-E.U.) and decreased thereafter. This may be explained by taking into account the effect of significant and continuous decrease of the absorption efficiency of this material with increasing peak voltage. This in turn is due to the low density and low effective atomic number of $\text{CaF}_2:\text{Eu}$ resulting in low light yield, when interacting with higher energy photons [46,61].

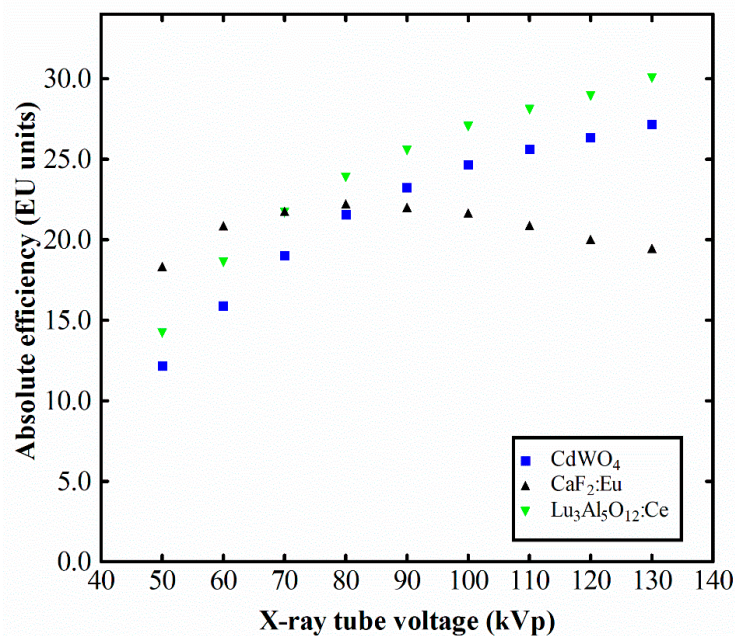


Figure 1. Luminescence efficiency of the CdWO_4 single crystal. Comparison with $\text{CaF}_2:\text{Eu}$ and $\text{Lu}_3\text{Al}_5\text{O}_{12}:\text{Ce}$ crystals.

Figure 2 shows the light output curves of CdWO_4 , $\text{CaF}_2:\text{Eu}$, and $\text{Lu}_3\text{Al}_5\text{O}_{12}:\text{Ce}$ single crystals, relating the light output signal with the incident X-ray exposure rate. A linear response can be depicted between the output LE and incident exposure in the examined range of exposures, with R^2 values higher than 0.9974 in all cases. The three curves followed the same trend with the luminescence efficiency results, in which CdWO_4 showed high light output values across the examined range, close to those of $\text{Lu}_3\text{Al}_5\text{O}_{12}:\text{Ce}$.

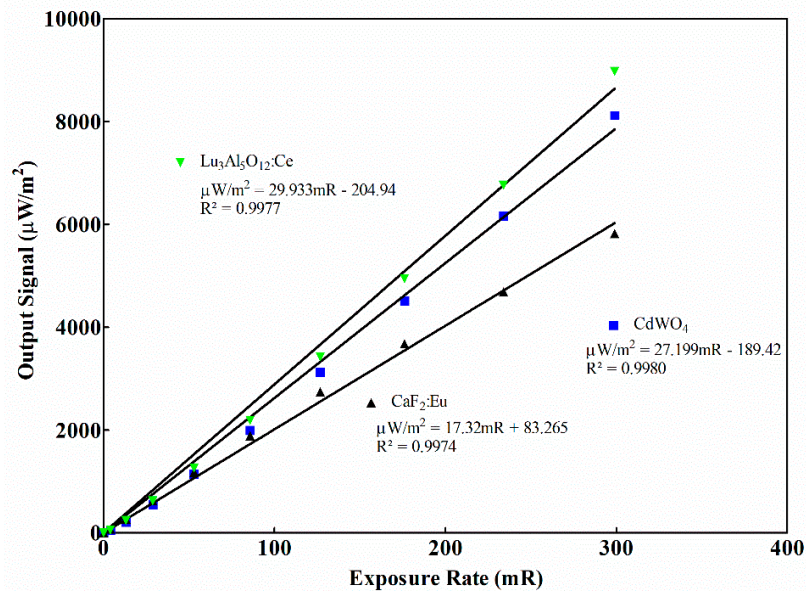


Figure 2. Output signal ($\mu\text{W}/\text{m}^2$) of the CdWO_4 single crystal. Comparison with $\text{CaF}_2:\text{Eu}$ and $\text{Lu}_3\text{Al}_5\text{O}_{12}:\text{Ce}$ crystals.

Figures 3–6 show the emitted light spectrum of the CdWO_4 crystal, obtained after irradiation using a UV lamp, along with the normalized spectral sensitivities of several optical sensors, across visible wavelengths [53–56]. The CdWO_4 spectrum shows the main luminescence peak at 490 nm (2.54 eV), associated with transitions in the tungstate group (WO_6) and a low intensity peak at about 595 nm (2.09 eV) [14,36,62].

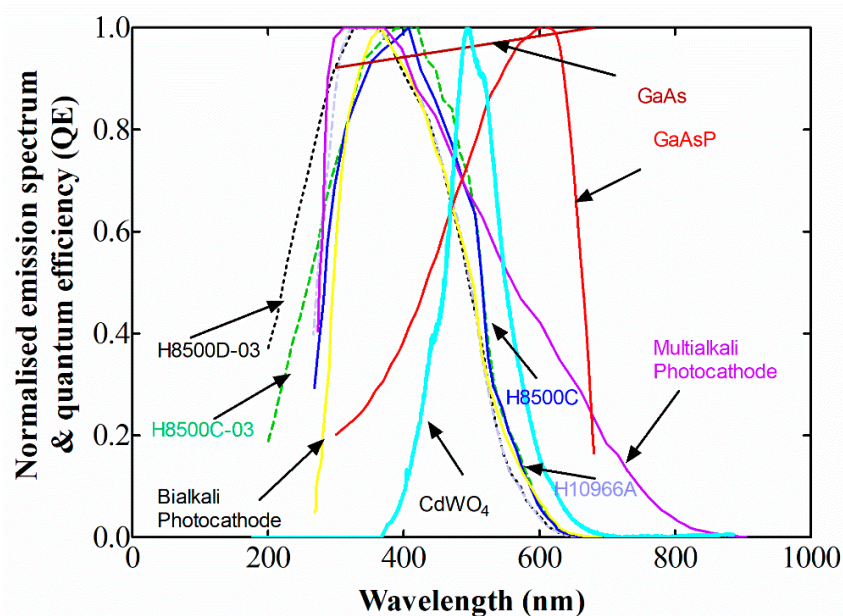


Figure 3. Light spectrum of CdWO_4 crystal along with the light sensitivity of various photocathodes.

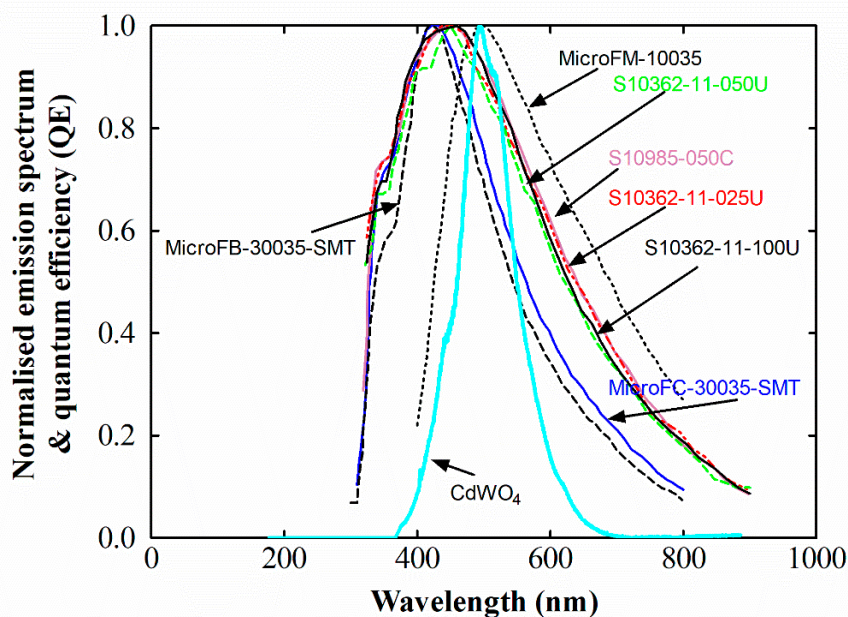


Figure 4. Light spectrum of CdWO₄ crystal along with the light sensitivity of various silicon photomultipliers.

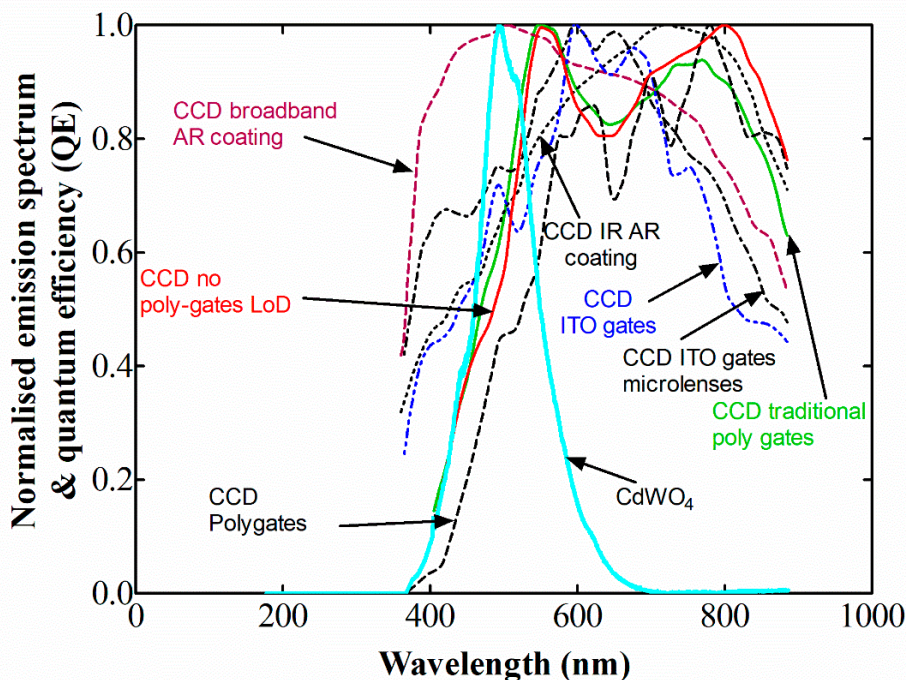


Figure 5. Light spectrum of CdWO₄ crystal along with the light sensitivity of various charge-coupled devices.

Table 2 shows spectral matching factor (SMF) values of the CdWO₄ with light sensors, such as PMT photocathodes, with position sensitive photomultipliers (PS-PMTs), silicon PMT (SiPMs), etc. The light emitted by the CdWO₄ scintillator shows an 85% overlap with the (E-S20) photocathode (SMF = 0.85) that was used in our experimental setup. This value was considered for correcting the luminescence efficiency measurements. CdWO₄ light makes a perfect match with CCD sensors (SMF = 0.97) and also with hydrogenated amorphous silicon (a-Si:H) photodiodes (SMF = 0.97). Furthermore, the SMF with photomultiplier photocathodes was also excellent, showing an SMF value of 0.96 with a gallium arsenide photocathode (GaAs).

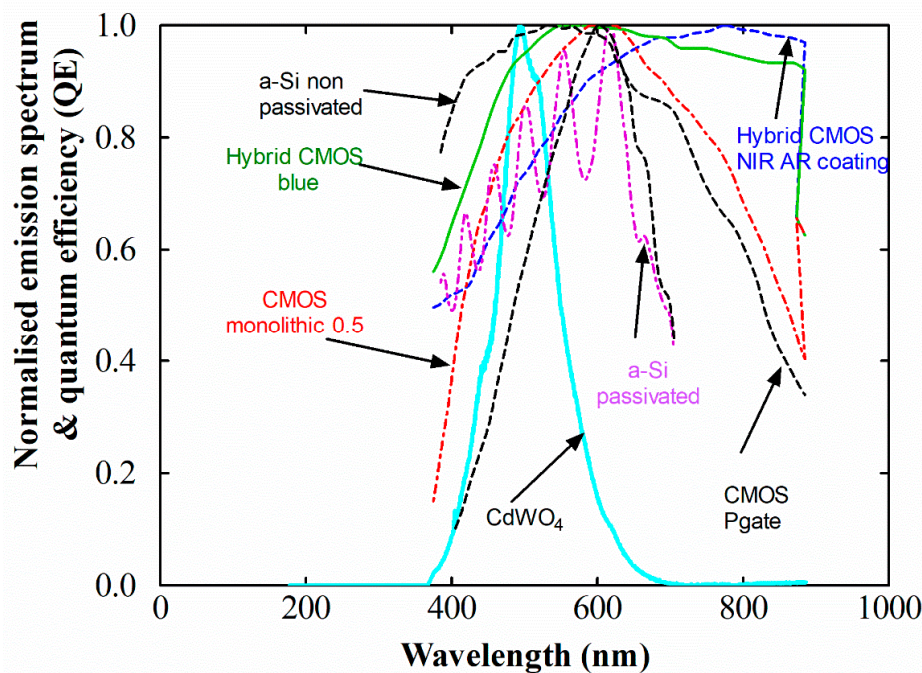


Figure 6. Light spectrum of CdWO₄ crystal along with the light sensitivity of various complementary metal–oxide semiconductors.

Table 2. Spectral matching values.

Optical Detectors	CdWO ₄	Optical Detectors	CdWO ₄
CCD broadband anti reflective coating	0.97	Photocathode GaAsP	0.76
CCD infrared anti-reflection coating	0.69	Photocathode E-S20	0.85
CMOS hybrid with blue anti-reflection coating	0.74	Si-PM MicroFC30035SMT	0.72
Hybrid CMOS blue emission	0.93	Si-PM MicroFB30035SMT	0.66
CMOS (monolithic 0.25 μm)	0.84	Si-PM MicroFM10035	0.88
passivated a-Si:H	0.75	Si-PM S10985050C	0.87
non-passivated a-Si:H	0.97	Si-PM S1036211025U	0.85
CCD with indium tin oxide gates and microlenses	0.78	Si-PM S1036211050U	0.87
CCD with indium tin oxide gates	0.68	Si-PM S1036211100U	0.86
CCD poly-gates	0.46	PS-PMT Flat panel H8500C03	0.56
CCD no poly-gates	0.66	PS-PMT Flat panel H8500D03	0.43
CCD traditional poly-gates	0.70	PS-PMT Flat panel H10966A	0.43
CMOS (photo-gate array)	0.60	PS-PMT Flat panel H8500C	0.53
CMOS Rad-Eye high resolution	0.82	Photocathode Bi-alkali	0.45
GaAs Photocathode	0.96	Photocathode Multi-alkali	0.64

CdWO₄ also showed good compatibility with a monolithic CMOS sensor (SMF = 0.84) and a high resolution RadEye CMOS (SMF = 0.82), used in medical and industrial radiography systems. With silicon photomultipliers, it showed SMF values in the range from 0.66 to 0.88 (MicroFM-10035 SMF = 0.88).

Figures 7–10 show LE values of the CdWO₄ as was effectively degraded by various optical detectors. These values are always less than the nominal light efficiency, since the matching of the light emitted by the examined crystals is registered differently by the various photodetectors due to their inherent light photon sensitivity. The optimum values for this study were obtained when CdWO₄ was coupled with a CCD with broadband AR coating and with an a-Si:H (non-passivated) photodiode. When silicon, or flat panel position sensitive photomultipliers, bi- or multi-alkali photocathodes are

used, having maximum detection efficiency in lower wavelengths (Figures 3, 4, 7 and 8), CdWO₄ shows higher SMF values, (ranging from 10.13% to 48.28%) compared to Lu₃Al₅O₁₂:Ce. This in turn results in higher effective efficiency (EE), showing the importance of this factor when designing an optical detection system. In detail, the increase (with kVp) in the detected luminescence signal ranged from 26.47% to 34.91% when CdWO₄ was coupled with the H10966A PS-PMT flat panel position sensitive photomultiplier, from 23.53% to 31.78% when CdWO₄ was coupled with the bi-alkali photocathode, and from 8.52% to 15.55% when CdWO₄ was coupled with the MicroFB-30035-SMT silicon photomultiplier, with respect to the corresponding values when these optical sensors were coupled to Lu₃Al₅O₁₂:Ce [47].

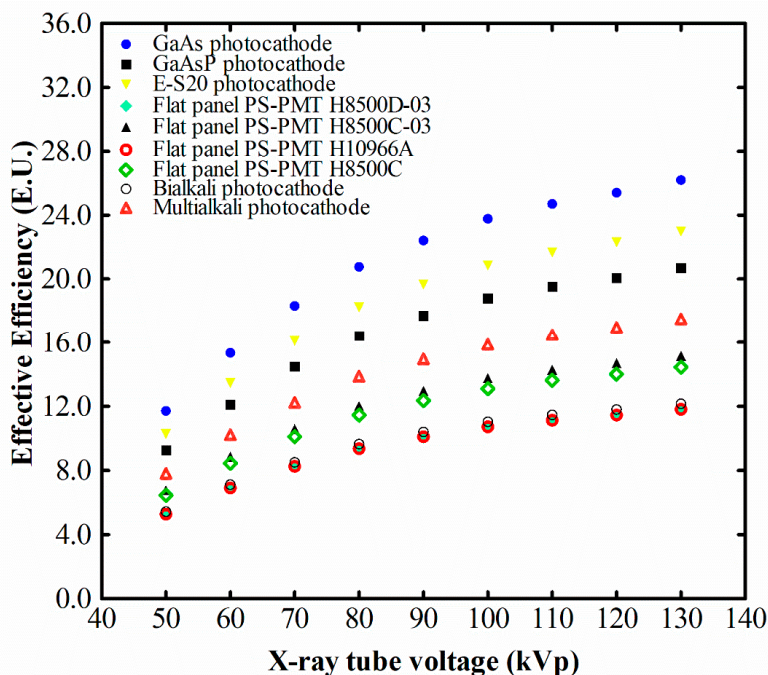


Figure 7. EE of CdWO₄ crystal with various photocathodes.

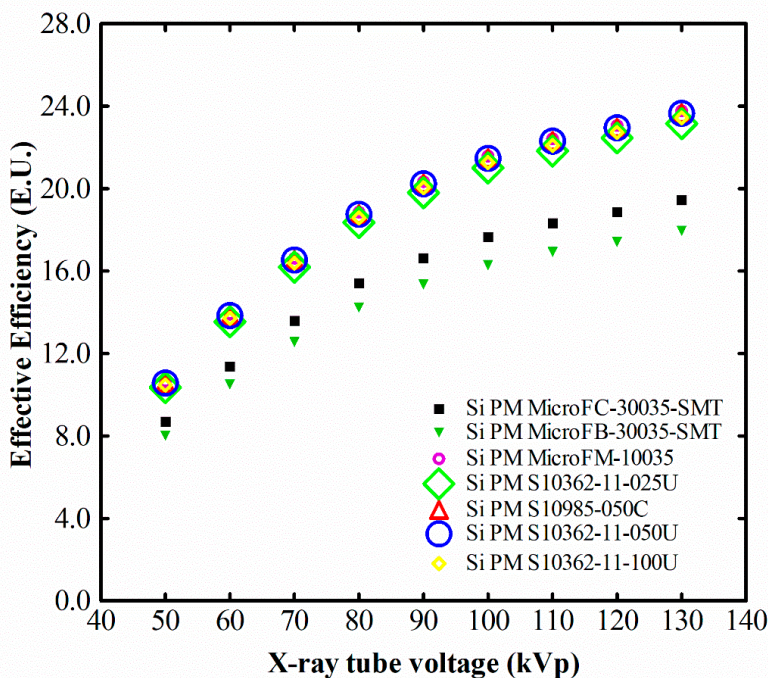


Figure 8. EE of CdWO₄ crystal with various silicon photomultipliers.

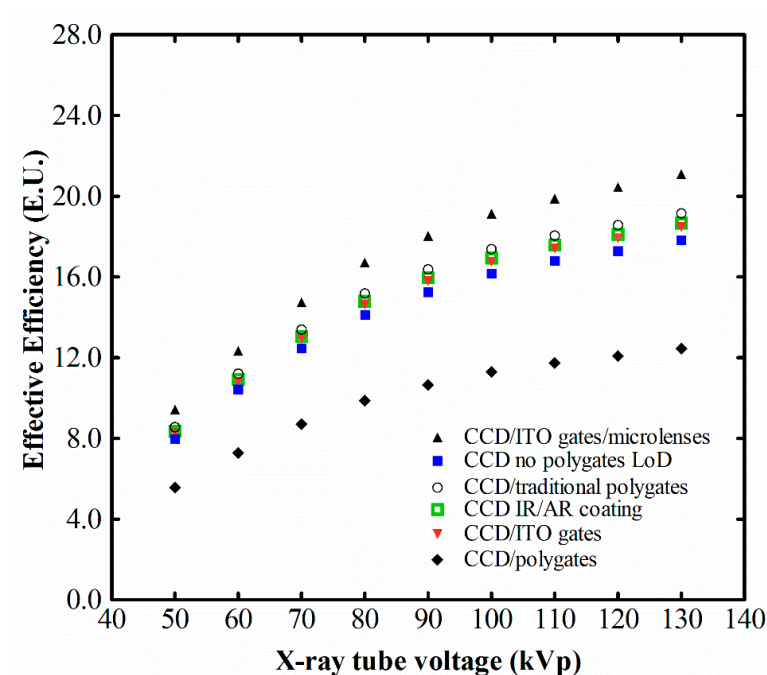


Figure 9. EE of CdWO₄ crystal with various charge-coupled devices.

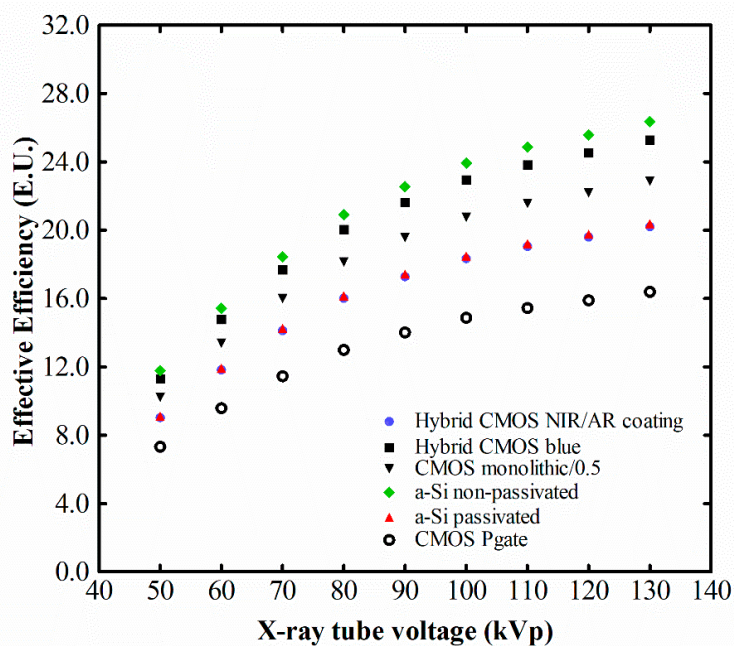


Figure 10. EE of CdWO₄ crystal with various complementary metal–oxide semiconductors.

Figure 11 illustrates the variation of calculated energy absorption efficiency values of the CdWO₄ in comparison with CaF₂:Eu and Lu₃Al₅O₁₂:Ce crystals of equal dimensions. The energy absorption efficiency of CdWO₄ was lower than that of both CaF₂:Eu and Lu₃Al₅O₁₂:Ce in the low-energy range (40 kVp) (0.67 for CdWO₄, 0.87 for Lu₃Al₅O₁₂:Ce and 0.82 for CaF₂:Eu crystals). Thereafter, CdWO₄ shows a tendency to increase up to 70 kVp (EAE = 0.73), and after 80 kVp, it shows higher EAE values than both CaF₂:Eu and Lu₃Al₅O₁₂:Ce crystals. The CaF₂:Eu crystal, having the lowest density value of 3.18 g/cm³, shows a clear tendency to decrease in the whole examined energy range. The higher density of CdWO₄ (CdWO₄ d = 7.9 g/cm³, Lu₃Al₅O₁₂:Ce d = 6.73 g/cm³) and the influence of the K-edge of the material (Figure 11 inset) contribute to the higher overall energy absorption efficiency values after 80 kVp.

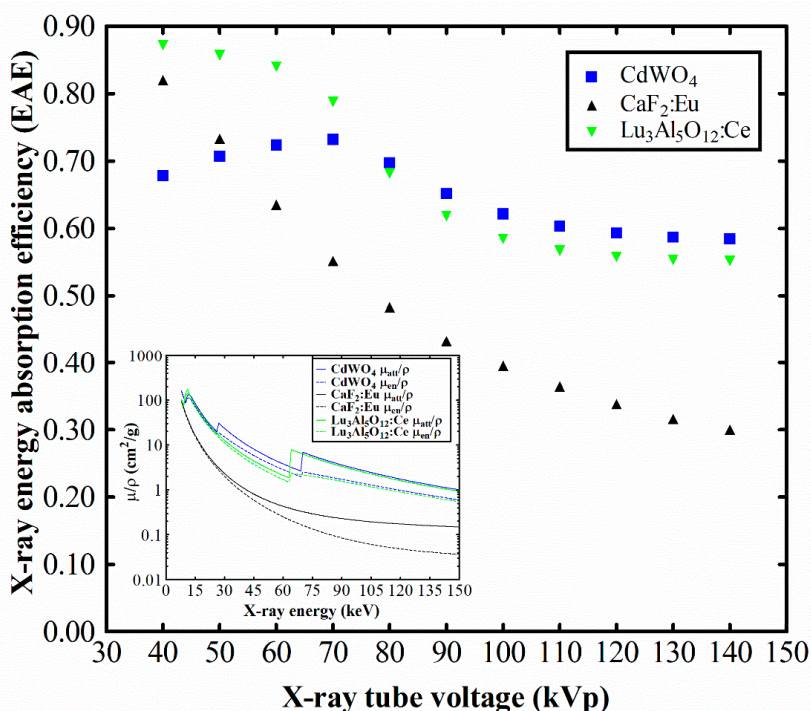


Figure 11. Energy absorption efficiency of the CdWO₄ single crystal. Comparison with CaF₂:Eu and Lu₃Al₅O₁₂:Ce. Inset: The corresponding X-ray coefficients.

Taking into consideration the absorption properties of CdWO₄, it would be of interest to mention previous relevant studies and possible applications. When high X-ray energies are considered, it has been previously demonstrated that for dual-energy applications, such as in material recognition imaging, the CsI-CdWO₄ dual detector combination performed sufficiently well when CdWO₄ acted as the high-energy component of the detector [63]. In diagnostic radiology X-rays, CdWO₄ has been studied as part of a Gd₂O₂S-CdWO₄ combination detector by Juste et al. [64] in the energy range from 10 to 160 keV and has been reported to exhibit adequate contrast between the low and the high-energy dual-energy spectral component. In addition, the ZnSe/CdWO combination has also been theoretically studied by Grinyov et al. [65] in 80–140 kV tube voltages. Finally, the two X-ray absorption edges of CdWO₄ at approximately 30 and 75 keV make it a suitable candidate for a dual-energy radiation detector either for single or double shot technique [66–68]. For single shot applications where the incident X-ray spectrum could be an 80 kVp filtered by 900 μm cerium (Ce) or a 90 kVp spectrum filtered with 2500 μm barium (Ba), which are presenting exposure peaks at the aforementioned energies, CdWO₄ would perform rather well [66–69]. Dual-energy applications are currently used in computed tomography (CT) systems in clinical practice. These can be regarded as either dual-energy or dual-source irradiation [70–72]. The X-ray tube voltages used are 80 kV (low-energy component) and 140 kV (high-energy component) [70–72], to satisfy the range of CT tube voltages [73]. As we can observe from Figure 1, at 80 kV, CdWO₄ is comparable to the CaF₂ scintillator, while for the higher kV energies, its efficiency characteristics are superior and present an increasing tendency. This may lead to improved signal to noise ratio (SNR) for the dual-energy CT high X-ray tube voltages, contributing to dose savings. The improved efficiency in high kV of CdWO₄ can be further exploited in dual-energy CT with a contrast agent [70,72], where in the low-energy region, the contrast-to-noise ratio is mainly affected by the contrast agent X-ray absorption characteristics, while in the high-energy part, a sensitive image detector can contribute to noise minimization through adequate dose management.

Dual-energy chest radiography improves the diagnostic value of an X-ray by separating soft tissue from bones, producing two different images using either a single or a double exposure technique. In the single exposure technique, two phosphor plates are exposed to X-rays, separated by a copper

filter. The front plate receives the unfractionated beam and produces a standard chest X-ray [74]. The high-energy photons are received by the back plate, while the lower energy photons are removed due to the front plate and copper filter. In the dual exposure technique [74–76], two images are obtained at different kVs, mainly at 60 and 120 kV [74,75], for the low and high energy, respectively. The resulting images are subtracted to produce the tissue-selective and bone-selective images. Although dual energy requires higher radiation doses, higher diagnostic accuracy can be achieved [74]. The higher X-ray energy absorption characteristics of CdWO_4 above 80 kV, as shown in Figure 11, make it a promising candidate for DE X-ray imaging that can contribute to dose saving when the high X-ray energy component is considered.

The use of crystalline scintillators in large detector arrays should address the problem of internal light scattering and crosstalk at the crystal edges [15,77]. The effect should be considered in positron emission tomography (PET) imaging and is affected by the photon energy [77]. When separated crystals are used, thickness separators, placed between the crystals, may be utilized to prevent the effect of internal light scattering and crosstalk. These separators should be thin and possess good reflectivity and low transparency [15]. A thin aluminum foil of 0.01 mm thickness has been reported to reduce light scatter [78]. In addition, 2D back illuminated photodiode arrays have been reported to adequately meet CT performance characteristics, including the effect of crosstalk, when large area CT detection systems are considered [79].

The differences between CdWO_4 and $\text{Lu}_3\text{Al}_5\text{O}_{12}:\text{Ce}$ in the tube voltage range of 40–70 kVp (Figure 11) can be explained by taking into account the ratios of the mass energy absorption coefficients over the total mass attenuation coefficients that are used for the EAE calculation, see Equation (3) and Figure 12. This range corresponds to energies of about 34–51 keV. From Figure 12, it can be seen that in the 34–51 keV energy range, the ratio of the mass energy absorption over the mass attenuation coefficients for $\text{Lu}_3\text{Al}_5\text{O}_{12}:\text{Ce}$ is higher than the corresponding ratio of CdWO_4 , despite the fact that the absolute values of mass energy absorption and the mass attenuation coefficients of CdWO_4 are higher in this range. Thereafter, the ratio of the coefficients for CdWO_4 is higher than that of $\text{Lu}_3\text{Al}_5\text{O}_{12}:\text{Ce}$, and this is reflected in EAE results of Figure 11. By contrast, $\text{CaF}_2:\text{Eu}$ starts with competitive values, in the low-energy range, but thereafter, the ratio of the coefficients is lower than for the other two materials, also resulting in lower EAE properties.

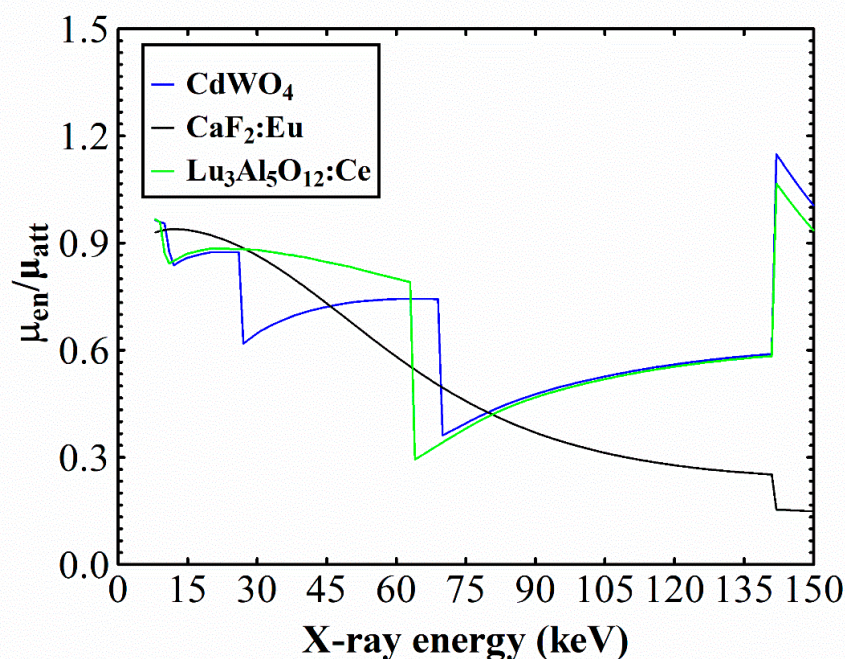


Figure 12. Ratio of the mass energy absorption coefficients over the total mass attenuation coefficients for the CdWO_4 , $\text{CaF}_2:\text{Eu}$ and $\text{Lu}_3\text{Al}_5\text{O}_{12}:\text{Ce}$ crystals.

4. Conclusions

The output luminescence signal of a CdWO₄ single crystal was examined within the radiographic energy region for possible applications in novel radiographic applications (such as dual energy). With this aim, the spectral compatibility with various commercial sensors was also considered. CaF₂:Eu and Lu₃Al₅O₁₂:Ce crystals of equal dimensions, were used in order to be compared with CdWO₄. The maximum luminescence efficiency was obtained at the maximum examined X-ray energy (130 kVp) since the output of the crystal constantly increased in the examined energy range. The emitted optical photons of CdWO₄ were found to be optimally detected by charge-coupled devices and amorphous hydrogenated silicon photodiodes employed in medical flat panel detectors. These values are perfectly matched for various imaging and non-imaging applications, such as dual-energy imaging, high-energy physics detectors, or applications of scintillators in harsh environments.

Author Contributions: Conceptualization, C.M. and G.F.; methodology, C.M., I.V., N.K., G.P and I.K.; software, V.K. and N.M.; validation, N.K. and G.P.; formal analysis, C.M., N.K., G.P. and I.S.; investigation, C.M., N.K., G.F., G.S. and I.G.; resources, A.B.; data curation, C.M., N.K., G.P., V.K., N.M., and I.K.; writing—original draft preparation, C.M.; writing—review and editing, I.K., N.K., V.K., N.M., G.P. and I.V.; visualization, C.M.; supervision, I.V.; project administration, C.M., and I.V.; funding acquisition, I.V. All authors have read and agreed to the published version of the manuscript.

Funding: The APC was funded by the Special Account for Research Grants, of the University of West Attica, Greece.

Conflicts of Interest: The authors declare no conflict of interest.

References

1. Ziluei, H.; Azimirad, R.; Larijani, M.; Ziaie, F. Preparation and optimization of CdWO₄-polymer nano-composite film as an alpha particle counter. *Nucl. Instrum. Methods Phys. Res. A* **2017**, *852*, 85–90. [[CrossRef](#)]
2. Kroger, F. *Some Aspects of Luminescence of Solids*; Elsevier Pub. Co.: Amsterdam, The Netherlands, 1948.
3. Kobayashi, M.; Ishii, M.; Usuki, Y.; Yahagi, H. Cadmium tungstate scintillators with excellent radiation hardness and low background. *Nucl. Instrum. Methods Phys. Res. A* **1994**, *349*, 407–411. [[CrossRef](#)]
4. Novais, S.; Da Silva, R.; Macedo, Z. Thermally stimulated luminescence of polycrystalline CdWO₄ at low temperatures. *J. Lumin.* **2011**, *131*, 1283–1287. [[CrossRef](#)]
5. Galashov, E.N.; Atuchin, V.V.; Kozhukhov, A.S.; Pokrovsky, L.D.; Shlegel, V.N. Growth of CdWO₄ crystals by the low thermal gradient Czochralski technique and the properties of a (010) cleaved surface. *J. Cryst. Growth.* **2014**, *401*, 156–159. [[CrossRef](#)]
6. Nagornaya, L.; Burachas, S.; Vostretsov, Y.; Martynov, V.; Ryzhikov, V. Studies of ways to reduce defects in CdWO₄ single crystals. *J. Cryst. Growth.* **1999**, *198/199*, 877–880. [[CrossRef](#)]
7. Sabharwal, S. Study of growth imperfections, optical absorption, thermoluminescence and radiation hardness of CdWO₄ crystals. *J. Cryst. Growth.* **1999**, *200*, 191–198. [[CrossRef](#)]
8. Ziluei, H.; Mojtahedzadeh, M.; Azimirad, L.; Ziaei, F. Fabrication of an alpha particle counter: Spin coated films of synthesized nanocrystalline cadmium tungstate powder. *Int. J. Radiat. Res.* **2017**, *15*, 425–430.
9. Shang, H.; Bliss, M.; Heald, S.; Sham, T.; Heigl, F.; Cao, G. Dense and optical transparent CdWO₄ films by sol-gel processing for scintillation applications. *J. Mater. Res.* **2007**, *22*, 1527–1536. [[CrossRef](#)]
10. Sofronov, D.; Sofronova, E.; Starikov, V.; Baymer, V.; Kudin, K.; Matejchenko, P.; Mamalis, A.; Lavrynenko, S. Microwave Synthesis of Tetragonal Phase CdWO₄. *Mater. Manuf. Process.* **2012**, *27*, 490–493. [[CrossRef](#)]
11. Nazarenko, B.; Baumer, V.; Dolzhenkova, E.; Kosmyna, M. Structural Defects in Czochralski-Grown CdWO₄ Single Crystals. *Inorg. Mater.* **2005**, *41*, 1114–1117. [[CrossRef](#)]
12. Ruiz-Fuertes, J.; Friedrich, A.; Errandonea, D.; Segura, A.; Morgenroth, W.; Rodríguez-Hernández, P.; Muñoz, A.; Meng, Y. Optical and structural study of the pressure-induced phase transition of CdWO₄. *Phys. Rev. B* **2017**, *95*, 174105. [[CrossRef](#)]
13. Babamoradi, M.; Liyai, M.; Azimirad, R.; Salehi, H. Electronic structure and optical properties of the single crystal and two-dimensional structure of CdWO₄ from first principles. *Phys. B Condens. Matter.* **2017**, *511*, 103–108. [[CrossRef](#)]

14. Grigorjeva, L.; Deych, R.; Millers, D.; Chernova, S. Time-resolved luminescence and absorption in CdWO₄. *Radiat. Meas.* **1998**, *29*, 267–271. [[CrossRef](#)]
15. Lecoq, P.; Gektin, A.; Korzhik, M. *Inorganic Scintillators for Detector Systems, Physical Principles and Crystal Engineering*, 2nd ed.; Springer: Switzerland, 2017.
16. Nagornaya, L.; Onyshchenko, G.; Pirogov, E.; Starzhinskiy, N.; Tupitsyna, I.; Ryzhikov, V.; Galich, Y.; Vostretsov, Y.; Galkin, S.; Voronkin, E. Production of the high-quality CdWO₄ single crystals for application in CT and radiometric monitoring. *Nucl. Instrum. Methods Phys. Res. A* **2005**, *537*, 163–167. [[CrossRef](#)]
17. Moszynski, M.; Balcerzyk, M.; Kapusta, M.; Syntfeld, A.; Wolski, D.; Pausch, G.; Stein, J.; Schotanus, P. CdWO₄ crystal in gamma-ray spectrometry. *IEEE Trans. Nucl. Sci.* **2005**, *52*, 3124–3312. [[CrossRef](#)]
18. Tupitsyna, I.; Grinyov, B.; Katrunov, K.; Nagornaya, L.; Onishchenko, G. Radiation Damage in CWO Scintillation Crystals with Different Defects. *IEEE Trans. Nucl. Sci.* **2009**, *56*, 2983–2988. [[CrossRef](#)]
19. Lammers, M.; Blasse, G.; Roberts, D. The Luminescence of Cadmium Tungstate (CdWO₄). *Phys. Stat. Sol. A* **1981**, *63*, 569–572. [[CrossRef](#)]
20. Chirila, M.; Garces, N.; Murphy, H.; Wicks, C.; Grencewicz, K.; Halliburton, L.; Giles, N. Identification of trapping sites for OH[−] molecular ions in CdWO₄. *J. Phys. Chem. Solids.* **2000**, *61*, 1871–1876. [[CrossRef](#)]
21. Garces, N.; Chirila, M.; Murphy, H.; Foise, J.; Thomas, E.; Wicks, C.; Grencewicz, K.; Halliburton, L.; Giles, N. Absorption, luminescence, and electron paramagnetic resonance of molybdenum ions in CdWO₄. *J. Phys. Chem. Solids.* **2003**, *64*, 1195–1200. [[CrossRef](#)]
22. Xu, W.; Zheng, C.; Hua, H.; Yang, Q.; Chen, L.; Xi, Y.; Hu, C. Synthesis and photoelectrochemical properties of CdWO₄ and CdS/CdWO₄ nanostructures. *Appl. Surf. Sci.* **2015**, *327*, 140–148. [[CrossRef](#)]
23. Eritenko, A.; Tsvetyansky, A. Separation of materials according to the effective atomic number using photons of two energies in the range of 60–700 keV. *Nucl. Instrum. Meth. Phys. Res. B* **2020**, *462*, 114–118. [[CrossRef](#)]
24. Gupta, T. *Radiation, Ionization, and Detection in Nuclear Medicine*; Springer-Verlag: Berlin, Germany, 2013.
25. Lecoq, P. Development of new scintillators for medical applications. *Nucl. Instrum. Methods Phys. Res. A* **2016**, *809*, 130–139. [[CrossRef](#)]
26. Van Eijk, C. Inorganic scintillators in medical imaging. *Phys. Med. Biol.* **2002**, *47*, R85–R106. [[CrossRef](#)] [[PubMed](#)]
27. Atuchin, V.; Galashov, E.; Khyzhun, O.; Bekenev, V.; Pokrovsky, L.; Borovlev, Y.; Zhdankov, V. Low Thermal Gradient Czochralski growth of large CdWO₄ crystals and electronic properties of (010) cleaved surface. *J. Solid State Chem.* **2016**, *236*, 24–31. [[CrossRef](#)]
28. Hosseinpour-Mashkani, S.; Sobhani-Nasab, A. A simple sonochemical synthesis and characterization of CdWO₄ nanoparticles and its photocatalytic application. *J. Mater. Sci. Mater. Electron.* **2016**, *27*, 3240–3244. [[CrossRef](#)]
29. Marsooli, M.; Fasihi-Ramandi, M.; Adib, K.; Pourmasoud, S.; Ahmadi, F.; Ganjali, M.; Sobhani Nasab, A.; Rahimi Nasrabadi, M.; Plonska-Brzezinska, M. Preparation and Characterization of Magnetic Fe₃O₄/CdWO₄ and Fe₃O₄/CdWO₄/PrVO₄. Nanoparticles and Investigation of Their Photocatalytic and Anticancer Properties on PANC1 Cells. *Materials* **2019**, *12*, 3274. [[CrossRef](#)]
30. Kosmyna, M.; Nazarenko, B.; Puzikov, V.; Shekhovtsov, A.; Ananenko, A.; Borodenko, Y.; Grinyov, B.; Koz'min, Y.; Tarasov, V. CdWO₄ crystal growth and production of a spectrometric detection unit with a large-volume ($V \cong 350 \text{ cm}^3$) crystal. *Crystallogr. Rep.* **2009**, *54*, 1265–1267. [[CrossRef](#)]
31. Grigoriev, D.; Danevich, F.; Shlegel, V.; Vasiliev, Y. Development of crystal scintillators for calorimetry in high energy and astroparticle physics. *J. Inst.* **2014**, *9*, C09004. [[CrossRef](#)]
32. Hojamberdiev, M.; Kanakala, R.; Ruzimuradov, O.; Yan, Y.; Zhu, G.; Xu, Y. Besom-like CdWO₄ structures composed of single-crystalline nanorods grown under a simple hydrothermal process in ultra-wide pH range. *Opt. Mater.* **2012**, *34*, 1954–1957. [[CrossRef](#)]
33. Rutherford, M.; Chapman, D.; White, T.; Drakopoulos, M.; Rack, A.; Eakins, D. Evaluating scintillator performance in time-resolved hard X-ray studies at synchrotron light sources. *J. Synchrotron. Radiat.* **2016**, *23*, 685–693. [[CrossRef](#)]
34. Martz, H.; Glenn, S.; Smith, J.; Divin, C.; Azevedo, S. Poly- Versus Mono-Energetic Dual-Spectrum Non-Intrusive Inspection of Cargo Containers. *IEEE Trans. Nucl. Sci.* **2017**, *64*, 1709–1718. [[CrossRef](#)]
35. Maddalena, F.; Tjahjana, L.; Xie, A.; Arramel, A.; Zeng, S.; Wang, H.; Coquet, P.; Drozdowski, W.; Dujardin, C.; Dang, C.; et al. Inorganic, Organic, and Perovskite Halides with Nanotechnology for High-Light Yield X- and γ -ray Scintillators. *Crystals* **2019**, *9*, 88. [[CrossRef](#)]

36. Nagirnyi, V.; Feldbach, E.; Jönsson, L.; Kirm, M.; Kotlov, A.; Lushchik, A.; Nagornaya, L.; Savikhin, F.; Svensson, G. Study of oriented CdWO₄ scintillating crystals using synchrotron radiation. *Radiat. Meas.* **2001**, *33*, 601–604. [CrossRef]
37. Brik, M.; Nagirnyi, V.; Kirm, M. Ab-initio studies of the electronic and optical properties of ZnWO₄ and CdWO₄ single crystals. *Mater. Chem. Phys.* **2012**, *134*, 1113–1120. [CrossRef]
38. Barabash, A.; Belli, P.; Bernabeib, R.; Borovlev, Y.; Cappella, F.; Caracciolo, V.; Cerulli, R.; Danevich, F.; Incicchitti, A.; Kobychiev, V.; et al. Improvement of radiopurity level of enriched ¹¹⁶CdWO₄ and ZnWO₄ crystal scintillators by recrystallization. *Nucl. Instrum. Methods Phys. Res. A* **2016**, *833*, 77–81. [CrossRef]
39. Grinyov, B.; Ryzhikov, V.; Lecoq, P.; Naydenov, S.; Opolonin, A.; Lisetskaya, E.; Galkin, S.; Shumeiko, N. Dual-energy radiography of bone tissues using ZnSe-based scintielectronic detectors. *Nucl. Instrum. Methods Phys. Res. A* **2007**, *571*, 399–403. [CrossRef]
40. Barthe, N.; Braillon, P.; Ducassou, D.; Basse-Cathalinat, B. Comparison of two Hologic DXA systems (QDR 1000 and QDR 4500/A). *Br. J. Radiol.* **1997**, *70*, 728–739. [CrossRef]
41. Panetta, D. Advances in X-ray detectors for clinical and preclinical Computed Tomography. *Nucl. Instrum. Methods Phys. Res. A* **2016**, *809*, 2–12. [CrossRef]
42. Martini, N.; Koukou, V.; Michail, C.; Fountos, G. Dual Energy X-ray Methods for the Characterization, Quantification and Imaging of Calcification Minerals and Masses in Breast. *Crystals* **2020**, *10*, 198. [CrossRef]
43. Popov, P.; Skrobov, S.; Zharikov, E.; Lis, D.; Subbotin, K.; Ivleva, L.; Shlegel, V.; Kosmyrna, M.; Shekhovtsov, A. Investigation of the Thermal Conductivity of Tungstate Crystals. *Crystallogr. Rep.* **2018**, *63*, 111–116. [CrossRef]
44. Advatech, U.K. Advatech-Radiation Detection/Imaging and Photonics. Available online: <https://www.advatech-uk.co.uk/index.html> (accessed on 20 March 2020).
45. Advatech, U.K. CdWO₄/CWO - Cadmium Tungstate. Available online: <https://www.advatech-uk.co.uk/cdwo4.html> (accessed on 20 March 2020).
46. Michail, C.; Kalyvas, N.; Bakas, A.; Ninos, K.; Sianoudis, I.; Fountos, G.; Kandarakis, I.; Panayiotakis, G.; Valais, I. Absolute Luminescence Efficiency of Europium-Doped Calcium Fluoride (CaF₂:Eu) Single Crystals under X-ray Excitation. *Crystals* **2019**, *9*, 234. [CrossRef]
47. Michail, C.; Ninos, K.; Kalyvas, N.; Bakas, A.; Saatsakis, G.; Fountos, G.; Sianoudis, I.; Panayiotakis, G.; Kandarakis, I.; Valais, I. Spectral Efficiency of Lutetium Aluminum Garnet (Lu₃Al₅O₁₂:Ce) with Microelectronic Optical Sensors. *Microelectron. Reliab.* **2020**, *109*, 113658. [CrossRef]
48. Michail, C.; Valais, I.; Martini, N.; Koukou, V.; Kalyvas, N.; Bakas, A.; Kandarakis, I.; Fountos, G. Determination of the Detective Quantum Efficiency (DQE) of CMOS/CsI Imaging Detectors following the novel IEC 62220-1-1:2015 International Standard. *Radiat. Meas.* **2016**, *94*, 8–17. [CrossRef]
49. Valais, I.; Kandarakis, I.; Nikolopoulos, D.; Sianoudis, I.; Dimitropoulos, N.; Cavouras, D.; Nomicos, C.; Panayiotakis, G. Luminescence efficiency of Gd₂SiO₅:Ce scintillator under x-ray excitation. *IEEE Trans. Nucl. Sci.* **2005**, *52*, 1830–1835. [CrossRef]
50. Saatsakis, G.; Kalyvas, N.; Michail, C.; Ninos, K.; Bakas, A.; Fountzoula, C.; Sianoudis, I.; Karpetas, G.E.; Fountos, G.; Kandarakis, I.; et al. Optical Characteristics of ZnCuInS/ZnS (Core/Shell) Nanocrystal Flexible Films Under X-ray Excitation. *Crystals* **2019**, *9*, 343. [CrossRef]
51. Michail, C.; Valais, I.; Fountos, G.; Bakas, A.; Fountzoula, C.; Kalyvas, N.; Karabotsos, A.; Sianoudis, I.; Kandarakis, I. Luminescence Efficiency of Calcium Tungstate (CaWO₄) under X-ray radiation: Comparison with Gd₂O₂S:Tb. *Measurement* **2018**, *120*, 213–220. [CrossRef]
52. Boone, J. X-ray production, interaction, and detection in diagnostic imaging. In *Handbook of Medical Imaging: Physics and Psychophysics*; Beutel, J., Kundel, H., Van Metter, R., Eds.; SPIE: Bellingham, WA, USA, 2000; Volume 1, pp. 36–57.
53. Hamamatsu Photonics, MPPC (Multi-Pixel Photon Counters). Available online: <http://www.hamamatsu.com/us/en/product/category/3100/4004/4113/index.html#> (accessed on 23 January 2020).
54. SensL, Silicon Photomultiplier. Available online: <https://www.onsemi.cn/PowerSolutions/resolveTaxonomy.do?url=/products/sensors/silicon-photomultipliers-sipm> (accessed on 23 January 2020).
55. Rowlands, J.A.; Yorkston, J. Flat Panel Detectors for Digital Radiography. In *Handbook of Medical Imaging Physics and Psychophysics*; Beutel, J., Kundel, H., Van Metter, R., Eds.; SPIE: Bellingham, WA, USA, 2000; Volume 1, pp. 223–328. ISBN 9780819477729.

56. Magnan, P. Detection of visible photons in CCD and CMOS: A comparative view. *Nucl. Instrum. Methods Phys. Res. A* **2003**, *504*, 199–212. [[CrossRef](#)]
57. Hubbell, J.; Seltzer, S. *Tables of X-ray Mass Attenuation Coefficients and Mass Energy Absorption Coefficients 1 to 20 MeV for Elements Z = 1 to 92 and 48 Additional Substances of Dosimetric interest*; NISTIR 5632; US Department of Commerce: Gaithersburg, MD, USA, 1995.
58. Storm, E.; Israel, H. *Report LA-3753*; Los Alamos Scientific Laboratory, University of California: Berkeley, CA, USA, 1967.
59. Evans, R.D. *The Atomic Nucleus*; McGraw-Hill: New York, NY, USA, 1955.
60. Seibert, J.; Boone, J. X-ray imaging physics for nuclear medicine technologists. Part 2: X-ray interactions and image formation. *J. Nucl. Med. Technol.* **2005**, *33*, 3–18.
61. Lina, L.; Leitnera, D.; Benattia, C.; Perdikakis, G.; Krausea, S.; Rencsoka, R.; Nasha, S.; Wittmer, W. Investigation of ion induced damage in KBr, YAG:Ce, CaF₂:Eu and CsI:Tl irradiated by various-energy protons. *J. Inst.* **2015**, *10*, P03024. [[CrossRef](#)]
62. Rzhevskaya, O.; Spasskii, D.; Kolobanov, V.; Mikhaelin, V.; Nagornaya, L.; Tupitsina, I.; Zadneprovskii, B. Optical and Luminescence Properties of CdWO₄ and CdWO₄:Mo Single Crystals. *Opt. Spectroscop.* **2008**, *104*, 366–373. [[CrossRef](#)]
63. Lee, K.; Natsui, T.; Hirai, S.; Uesaka, M.; Hashimoto, E. Application of X-Band Linac for Material Recognition with two Fold Scintillator Detector. In Proceedings of the Linear Accelerator Conference LINAC2010, Tsukuba, Japan, 12–17 September 2010; pp. 124–126.
64. Juste, B.; Morera, D.; Miró, R.; Verdú, G. Calculation of energetic dual-energy detector efficiency using MCNP and GEANT Monte Carlo codes. In Proceedings of the 2nd International Conference on Advancements in Nuclear Instrumentation, Measurement Methods and their Applications, Ghent, Belgium, 6–9 June 2011; pp. 1–4.
65. Grinyov, B.; Ryzhikov, V.; Naydenov, S.; Opolonin, A.; Lisetskaya, E.; Galkin, S.; Lecoq, P. Medical dual-energy imaging of bone tissues using ZnSe-based scintillator-photodiode detectors. *2006 IEEE Nucl. Sci. Symp. Conf. Rec.* **2006**, *3*, 1945–1949.
66. Koukou, V.; Martini, N.; Fountos, G.; Michail, C.; Sotiropoulou, P.; Bakas, A.; Kalyvas, N.; Kandarakis, I.; Speller, R.; Nikiforidis, G. Dual energy subtraction method for breast calcification imaging. *Nucl. Instrum. Methods Phys. Res. A* **2017**, *848*, 31–38. [[CrossRef](#)]
67. Koukou, V.; Martini, N.; Fountos, G.; Michail, C.; Bakas, A.; Oikonomou, G.; Kandarakis, I.; Nikiforidis, G. Application of a dual energy X-ray imaging method on breast specimen. *Result. Phys.* **2017**, *7*, 1634–1636. [[CrossRef](#)]
68. Martini, N.; Koukou, V.; Fountos, G.; Michail, C.; Bakas, A.; Kandarakis, I.; Speller, R.; Nikiforidis, G. Characterization of breast calcification types using dual energy x-ray method. *Phys. Med. Biol.* **2017**, *62*, 7741–7764. [[CrossRef](#)] [[PubMed](#)]
69. Martini, N.; Koukou, V.; Michail, C.; Sotiropoulou, P.; Kalyvas, N.; Kandarakis, I.; Nikiforidis, G.; Fountos, G. Pencil beam spectral measurements of Ce, Ho, Yb and Ba powders for potential use in Medical applications. *J. Spectrosc.* **2015**, *2015*, 563763. [[CrossRef](#)]
70. Yeh, B.; Shepherd, J.; Wang, Z.; Teh, H.; Hartman, R.; Prevrhal, S. Dual Energy and Low KVp CT in the Abdomen. *Am. J. Roentgenol.* **2009**, *193*, 47–54. [[CrossRef](#)]
71. Goodsitt, M.; Christodoulou, E.; Larson, S. Accuracies of the synthesized monochromatic CT numbers and effective atomic numbers obtained with a rapid kVp switching dual energy CT scanner. *Med. Phys.* **2011**, *38*, 2222–2232. [[CrossRef](#)]
72. Coursey, C.; Nelson, R.; Boll, D.; Paulson, E.; Ho, L.; Neville, A.; Marin, D.; Gupta, R.; Schindera, S. Dual-Energy Multidetector CT: How Does It Work, What Can It Tell Us, and When Can We Use It in Abdominopelvic Imaging? *RadioGraphics* **2010**, *30*, 1037–1055. [[CrossRef](#)]
73. Aichinger, H.; Dierker, J.; Joite-Barfuß, S.; Säbel, M. *Radiation Exposure and Image Quality in X-ray Diagnostic Radiology, Physical Principles and Clinical Applications*, 2nd ed.; Springer-Verlag: Berlin/Heidelberg, Germany, 2012; ISBN 987-3-642-11240-9.
74. Manji, F.; Wang, J.; Norman, G.; Wang, Z.; Koff, D. Comparison of dual energy subtraction chest radiography and traditional chest X-rays in the detection of pulmonary nodules. *Quant. Imaging Med. Surg.* **2016**, *6*, 1–5.

75. Shkumat, N.A.; Siewerdsen, J.H.; Dhanantwari, A.C.; Williams, D.B.; Richard, S.; Paul, N.S.; Yorkston, J.; Van Metter, R. Optimization of image acquisition techniques for dual-energy imaging of the chest. *Med. Phys.* **2007**, *34*, 3904–3915. [[CrossRef](#)]
76. Lee, M.; Lee, D.; Kim, H.; Choi, S.; Kim, D.; Kim, H.J. Development of a non-linear dual-energy technique in chest radiography. *Radiat. Phys. Chem.* **2020**, *172*, 108811. [[CrossRef](#)]
77. Zhang, C.; Sang, Z.; Wang, X.; Zhang, X.; Yang, Y. The effects of inter-crystal scattering events on the performance of PET detectors. *Phys. Med. Biol.* **2019**, *64*, 205004. [[CrossRef](#)] [[PubMed](#)]
78. Fritz, S.; Cook, L. High-resolution digital x-ray detector utilizing a discrete array of CdWO₄ scintillators and a self-scanned photodiode array. *Med. Phys.* **1987**, *14*, 244–248. [[CrossRef](#)] [[PubMed](#)]
79. Luhta, R.; Mattson, R.; Taneja, N.; Bui, P.; Vasbo, R. Back-illuminated photodiodes for multislice CT. In Proceedings of the SPIE 5030, Medical Imaging 2003: Physics of Medical Imaging, San Diego, CA, USA, 5 June 2003. [[CrossRef](#)]



© 2020 by the authors. Licensee MDPI, Basel, Switzerland. This article is an open access article distributed under the terms and conditions of the Creative Commons Attribution (CC BY) license (<http://creativecommons.org/licenses/by/4.0/>).